Simulating the Radiation Loss of Superconducting Submillimeter Wave Filters and Transmission Lines Using Sonnet EM

Endo, A.; Pascual Laguna, A.; Hähnle, S.; Karatsu, K.; Thoen, D. J.; Murugesan, V.; Baselmans, J.J.A.

Citation (APA)
Endo, A., Pascual Laguna, A., Hähnle, S., Karatsu, K., Thoen, D. J., Murugesan, V., & Baselmans, J. J. A. (2020). Simulating the Radiation Loss of Superconducting Submillimeter Wave Filters and Transmission Lines Using Sonnet EM. In J. Zmuidzinas, & J.-R. Gao (Eds.), *Millimeter, Submillimeter, and Far-Infrared Detectors and Instrumentation for Astronomy X* (Vol. 11453, pp. 436 - 447). Article 114532T (Proceedings of SPIE - The International Society for Optical Engineering; Vol. 11453). SPIE. https://doi.org/10.1117/12.2560458

Important note
To cite this publication, please use the final published version (if applicable).
Please check the document version above.

PROCEEDINGS OF SPIE

Simulating the radiation loss of superconducting submillimeter wave filters and transmission lines using Sonnet EM

Endo, Akira, Pascual Laguna, Alejandro, Hähnle, Sebastian, Karatsu, Kenichi, Thoen, David, et al.

SPIE.

Simulating the radiation loss of superconducting submillimeter wave filters and transmission lines using Sonnet EM

Akira Endo[a,b,*], Alejandro Pascual Laguna[a,c], Sebastian Hähnle[a,c], Kenichi Karatsu[a,c], David J. Thoen[a], Vignesh Murugesan[c], and Jochem J.A. Baselmans[a,c]

[a]Faculty of Electrical Engineering, Mathematics and Computer Science, Delft University of Technology, Mekelweg 4, 2628 CD Delft, the Netherlands.
[b]Kavli Institute of NanoScience, Faculty of Applied Sciences, Delft University of Technology, Lorentzweg 1, 2628 CJ Delft, The Netherlands.
[c]SRON—Netherlands Institute for Space Research, Sorbonnelaan 2, 3584 CA Utrecht, The Netherlands.

ABSTRACT

Superconducting resonators and transmission lines are fundamental building blocks of integrated circuits for millimeter-submillimeter astronomy. Accurate simulation of radiation loss from the circuit is crucial for the design of these circuits because radiation loss increases with frequency, and can thereby deteriorate the system performance. Here we show a stratification for a 2.5-dimensional method-of-moment simulator Sonnet EM that enables accurate simulations of the radiative resonant behavior of submillimeter-wave coplanar resonators and straight coplanar waveguides (CPWs). The Sonnet simulation agrees well with the measurement of the transmission through a coplanar resonant filter at 374.6 GHz. Our Sonnet stratification utilizes artificial lossy layers below the lossless substrate to absorb the radiation, and we use co-calibrated internal ports for de-embedding. With this type of stratification, Sonnet can be used to model superconducting millimeter-submillimeter wave circuits even when radiation loss is a potential concern.

Keywords: Kinetic Inductance Detectors, Millimeter-wave, Submillimeter-wave, DESHIMA, Integrated Superconducting Spectrometer, Simulation, Coplanar Waveguide, Astronomical Instrumentation

1. INTRODUCTION

Superconducting microwave resonators are used in astronomical instrumentation,[1–3] quantum computation[4,5] and solid state physics.[6] For designing the resonators and the superconducting transmission line circuit around it, the planar method of moment (MoM) simulation software Sonnet em[7] (Sonnet, hereafter) is widely used. This is because Sonnet requires less simulation time compared to full 3D simulators (e.g., CST Microwave Studio[8] and HFSS[9]) for planar structures,[10] and it is straightforward to model superconductors in Sonnet.[11,12]

In recent years, there is an increasing demand in astronomical instrumentation for superconducting circuits that operate in the millimeter-submillimeter (mm-submm) band up to 1 THz.[1,13] At above ∼100 GHz, radiation losses become significant for coplanar structures, and the quality factor of resonators can deteriorate.[14] Whilst full 3D simulators can simulate free-space boundaries, Sonnet requires a perfect electrical conductor (PEC) surface on the four walls perpendicular to the planar structures. This can lead to problems such as suppression of radiative modes, reflections from the walls back to the circuit, and standing waves. Recently it has been reported that the radiation loss of a straight coplanar waveguide (CPW) can be accurately modeled with Sonnet by using a box that is sufficiently large to allow all radiative modes to be excited, and a stratification that prevents reflection from the walls of the simulation box.[11] Here we present the details of such a simulation, and show that the same stratification can also be applied to account for radiation loss in Sonnet simulations of

---

submillimeter wave resonators. We do this by comparing Sonnet simulations with experiments, and a simulation using CST Microwave Studio (CST, hereafter).

For the Sonnet simulations we have used Sonnet Version 17.56 on a Windows Server 2019 workstation with two AMD EPYC 7302 16-core processors (3.0 GHz), with hyper-threading (64 threads in total), and 512 GB of random access memory (16×36 GB).

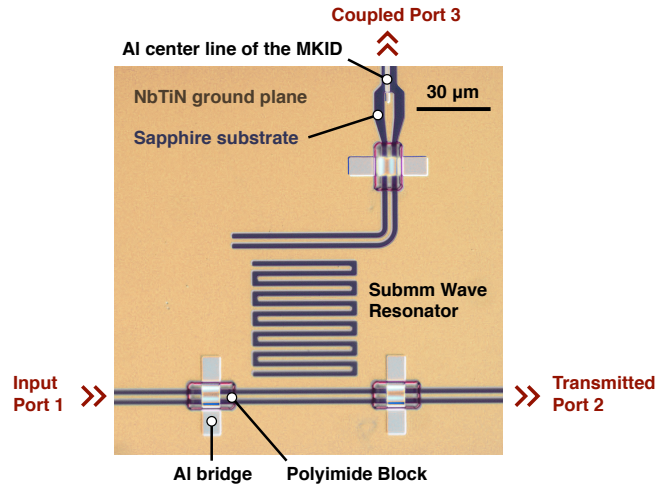## 2. SUPERCONDUCTING SUBMILLIMETER WAVE RESONATOR

Figure 1. Micrograph of the 374.6 GHz superconducting resonator.[14]

We will study the submm wave resonator shown in Fig. 1. The resonator is a meandering slotline patterned in the superconducting NbTiN ground plane on a c-plane sapphire substrate. The second harmonic mode of this resonator at 374.6 GHz is used as one of the bandpass filters in a filter bank circuit of the astronomical spectrometer DESHIMA (Deep Spectroscopic High-redshift Mapper).[14] At this frequency, the filter intercepts the submm wave signal flowing from the input port 1 to the transmission port 2, so that part of the signal is directed to the coupled port 3. The power sent to the coupled port 3 is measured with a microwave kinetic inductance detector (MKID). A previous study[14] of this resonator has shown that, at the resonance frequency, ~13% of the power from the input is radiated into the substrate. This radiative behavior makes it challenging to reproduce these results using Sonnet.
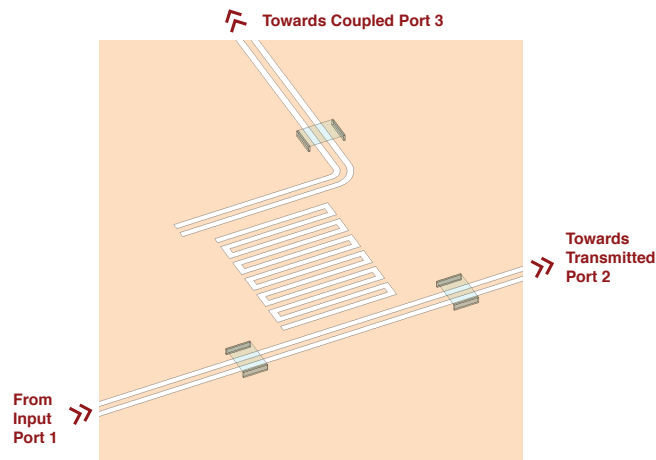

Figure 2. Design of the submm resonator in Sonnet. The three CPW lines extend to the edge of the ground plane, where they are terminated with an impedance-matched port.

In Fig. 2 we show the model of the resonator in Sonnet. All slots in the NbTiN film are 2-µm wide. The 100-nm thick NbTiN film is modeled as a metal sheet with a surface inductance of 1.0 pH/$\square$, calculated from the resistivity (102 $\mu\Omega$ cm), critical temperature (14.7 K), and thickness (100 nm) of a NbTiN film deposited in an identical manner.[11] (Note that the calculation of the surface inductance requires the full Mattis-Bardeen equations, and not the low-frequency limit of $L_\mathrm{s} = R_\mathrm{s}\hbar/(\pi\Delta)$, where R_s is the sheet resistance, $\hbar$ is the reduced Planck constant, and Δ is the superconducting gap energy.) The polyimide blocks under the aluminium bridges have been replaced with a vacuum layer to save computation time. The aluminium film used for the bridges is modeled as a metal sheet with a surface resistance of 0.63 $\Omega/\square$. The CPW lines have a characteristic impedance of 93 Ω. The CPW lines extend straight to the ports loaded with a matched impedance. The sapphire substrate is modeled with an anisotropic permittivity of 9.3 in the horizontal directions, and 11.9 in the vertical direction.
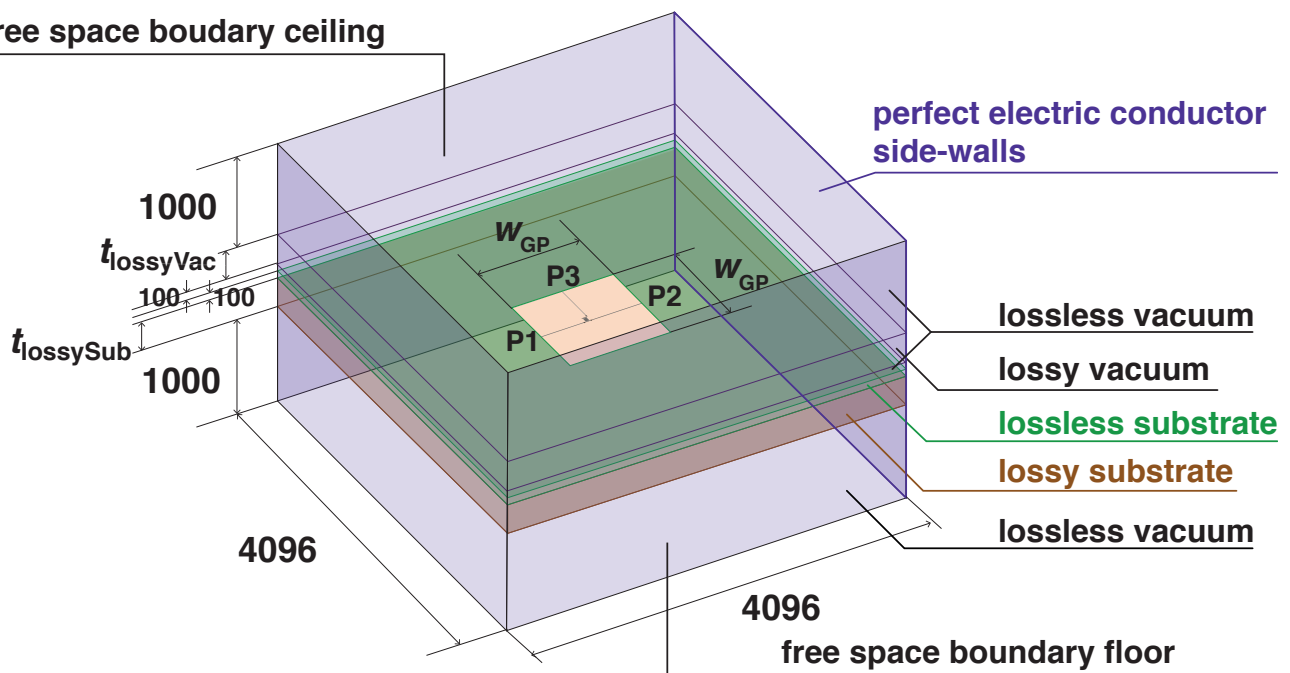
3. SONNET STRATIFICATION

3.1 Box

Figure 3. Stratification for the Sonnet simulation.

Fig. 3 shows the stratification of the ground plane, dielectric layers and the box around the resonator. In Sonnet, the four sidewalls of the box must be made of PEC. The ceiling and floor are set to the 'free space' boundary condition. In the horizontal directions, the box is 4096 µm by 4096 µm wide. The box is much larger than the metallization, for the following reasons:

1. When the sidewalls are close to each other, the box behaves like a rectangular waveguide. This means that radiation from the structure will be restricted to the set of discrete waveguide modes. This can lead to suppression of radiative modes that can be excited if the structure were placed in an infinite space. The typical scale recommended in the *Sonnet User's Guide* is one or two times the wavelength.[7]

2. When the sidewalls are not far enough from the structure, the radiation can be reflected at the walls and couple back into the structure. To prevent this, there must be sufficient attenuation of the signal between the structure and the walls. When standing waves are observed in the current distribution, this is a strong indication that there is significant reflection.

3. The area of the ground plane is kept to the minimum, because the calculation time of Sonnet scales roughly with the number of metal subsections cubed.[10]

In order to model an infinite space seen by the structure, we have introduced: 1) a double-layer substrate that is designed to absorb the radiated power without affecting the waves in the resonator and CPWs. Directly under the NbTiN film layer, there is a 100-µm thick layer of sapphire with no dissipative loss. The thickness of 100 µm is much larger than the slot width of 2 µm, ensuring that all the guided waves (near field) are contained in this layer. Under this lossless substrate, there is an artificial lossy substrate which has the same anisotropic permittivity of c-plane sapphire and a loss tangent of $\tan \delta = 0.1$. The small difference in complex permittivity between the lossless and lossy layers ensures that there is little reflection at the interface. The thickness of the lossy substrate, t_{lossy}, will be chosen so that the signal radiated from the circuit is strongly attenuated and is not reflected back to the structure. For the same reason, we have also placed an artificial layer of lossy vacuum at 100 µm above the ground plane layer to absorb radiation that is launched above the substrate, depending on the circuit that is modeled. As we show in subsection 4.5, this layer has no effect for the cases simulated in this paper. Finally, above the lossy vacuum layer and below the lossy substrate, there are 1-mm thick layers of lossless vacuum that separate the lossy layers from the free-space boundaries at the top and bottom of the box.

3.2 Ports

Here we use 'co-calibrated internal ports', because this type of port can be placed on the edge of a metal that is not attached to the Sonnet box. (The most commonly used 'box-wall port' must be attached to the box wall.) The co-calibrated internal ports are de-embedded, so the results are accurate.[7] For our simulations we apply a 'floating' ground node connection, which internally creates a 'Generalized Local Ground' (GLG) metal connection at every port.[7] This GLG metal is removed in the de-embedding process. The short calibration length of 6 µm follows from a private discussion with Sonnet, but it is not studied in detail by us.

4. RESULTS

4.1 'Reference' Geometry

t_{lossySub}	10^2 µm
t_{lossyVac}	10^2 µm
$\tan \delta$	10^{-1}
w_{GP}	1024 µm
Δ_x	0
Δ_y	0
box size	4096 µm $\times$ 4096 µm

Table 1. Parameters defining the *reference* geometry. t_{lossySub} and t_{lossyVac} are the thicknesses of the artificial lossy layers in vacuum and below the substrate, respectively (see Fig. 3). $\tan \delta$ is the loss tangent of those layers. w_{GP} is the width of the ground plane (see Fig. 3). Δ_x and Δ_y are the offsets of the resonator position, see Fig. 6. Box size is the lateral dimension of the box (see Fig. 3).

We will first discuss the *reference* geometry, of which the parameters are listed in Table 1. The *reference* geometry is chosen as a good compromise between accuracy and calculation time. The resonator is placed close to the center of the ground plane, which is 1024 µm wide in both x and y directions. As mentioned earlier, for the NbTiN film in Sonnet we took a sheet inductance of 1.0 pH/□ that is derived from measured film properties. However, we adjust the sheet inductance in CST to 0.73 pH/□ to get the resonance frequency close to the measurement. The exact reason for the different sheet inductance required in CST is not clear at the time of publication. Furthermore, in order to align the simulated resonance frequency to the measurement, we multiplied the Sonnet frequency by a factor of 1.0067, and the CST frequency by a factor of 0.9986. *

The S-parameters calculated with Sonnet are compared with CST and measurements in Fig. 4. Because we can obtain only $|S_{31}|^2$ from the measurements, we take $|S_{31}|^2$ as the prime indicator for the accuracy of the

---

*This was much easier than iterating the simulations with varying sheet inductance to reach virtually the same result.
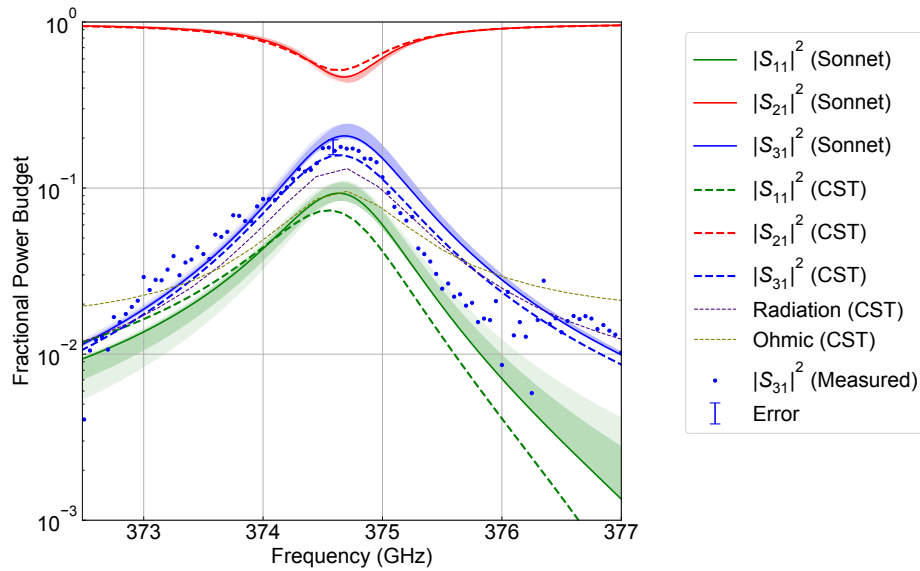
Figure 4. Fractional power budget as a function of frequency calculated by Sonnet (solid curves) using the *reference* geometry, compared to the result of CST (dashed curves) and measurement[14] (points). Shaded regions which indicate the maximum-minimum range of $|S_{n1}|^2$ curves calculated with position offsets indicated in Fig. 6 and Table 2. The thicker shading indicates the central 3×3 locations, and the thinner shading indicates all 5×5 locations.
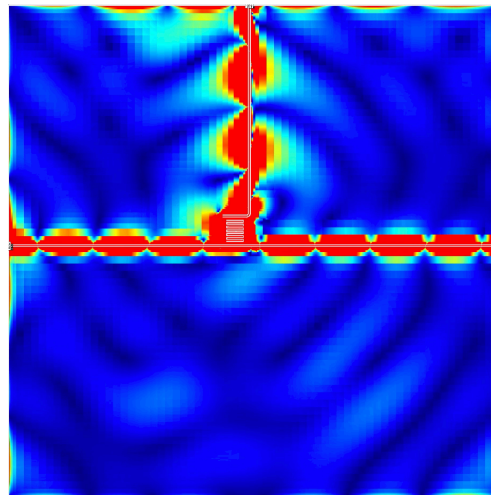

Figure 5. Snapshot of the current distribution J_{xy} for the *reference* geometry (▶ online video). Note that the current densities plotted do not represent de-embedded data, and therefore areas near any port include the effect of the port discontinuity, according to the manual of Sonnet.[15]

simulations. Both $|S_{31}|^2$ curves of Sonnet and CST are within the 1σ error range of the measurement[14] at the resonance peak.

The time-evolution of the current is a good indication of the presence of standing waves in the simulation box. Fig. 5 is a snapshot of an animation (▶ online video). The radiation leaving the resonator is not returning to the CPW, and there are no obvious indications of standing waves. (Typically, standing waves are visible if the box is too small, there is not enough dissipation in the box, etc.)
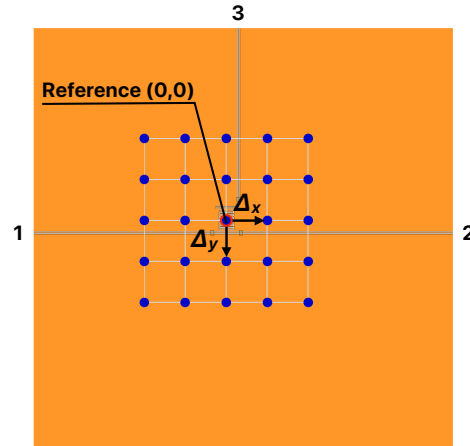
Figure 6. Locations of the *reference* and offset positions on the 1024 µm × 1024 µm ground plane. The numbers 1–3 indicate the location of the ports.

t_{lossySub}	10^2 µm
t_{lossyVac}	10^2 µm
$\tan\delta$	10^{-1}
w_{GP}	1024 µm
Δ_x	$-200, -100, \mathbf{0}, +100, +200$ µm
Δ_y	$-200, -100, \mathbf{0}, +100, +200$ µm
box size	4096 µm × 4096 µm

Table 2. Parameters defining the set of geometries used to test the sensitivity to offsets of the resonator within the ground plane. Bold characters indicate the *reference* geometry.

4.2 Sensitivity to offsets of the resonator within the ground plane

In Fig. 4 we show the effect of shifting the position of the resonator within the ground plane as indicated in Fig. 6 and Table 2. When we take the peak value of $|S_{31}|^2$, the ratio between maximum and minimum of all positions is 1.24, giving an indication of the accuracy of the Sonnet simulation.

Interestingly, the *reference* position located near the center of the ground plane (hence also the center of the simulation box) yields a peak $|S_{31}|^2$ that is the lowest among all positions. This could be an indication that there remains an effect of a finite distance to the box wall or the ground plane edge. Further investigation in the directions of:

1. moving the ground plane together with the resonator inside the box and comparing the effect, and

2. repeating the simulation with larger box sizes and larger ground plane sizes

are recommended if one would want to further improve the simulation accuracy.

4.3 Sensitivity to the ground plane width

The size of the ground plane can, in general, affect the amount of radiation loss. Here we keep the square shape of the ground plane and vary the length of the sides w_{GP} from 512 µm to 2048 µm, as summarized in Table 3. The result is shown in Fig. 7. Compared to the *reference* geometry ($w_{\text{GP}} = 1024$ µm), all other values for w_{GP} yield a slightly higher peak $|S_{31}|^2$ value. In general we expect that the larger the ground plane the more accurate the results are, because we are trying to simulate an infinite ground plane case. However, it should be noted that the experiment was also not with an infinite ground plane; there were neighboring filter channels on both sides of the filter at a distance of $3\lambda/4$. The $|S_{31}|^2$ peak of the smallest and hence least accurate $w_{\text{GP}} = 512$ µm geometry has a $|S_{31}|^2$ peak that is 22% higher than the *reference*. The $|S_{31}|^2$ peak of the largest, $w_{\text{GP}} = 2048$ µm geometry has a $|S_{31}|^2$ peak that is 13% higher than the *reference*.

t_{lossySub}	10^2 µm
t_{lossyVac}	10^2 µm
$\tan \delta$	10^{-1}
w_{GP}	512, **1024**, 1536, 2048 µm
Δ_x	0
Δ_y	0
box size	4096 µm $\times$ 4096 µm

Table 3. Parameters defining the set of geometries used to test the sensitivity to the ground plane width. Bold characters indicate the *reference* geometry.
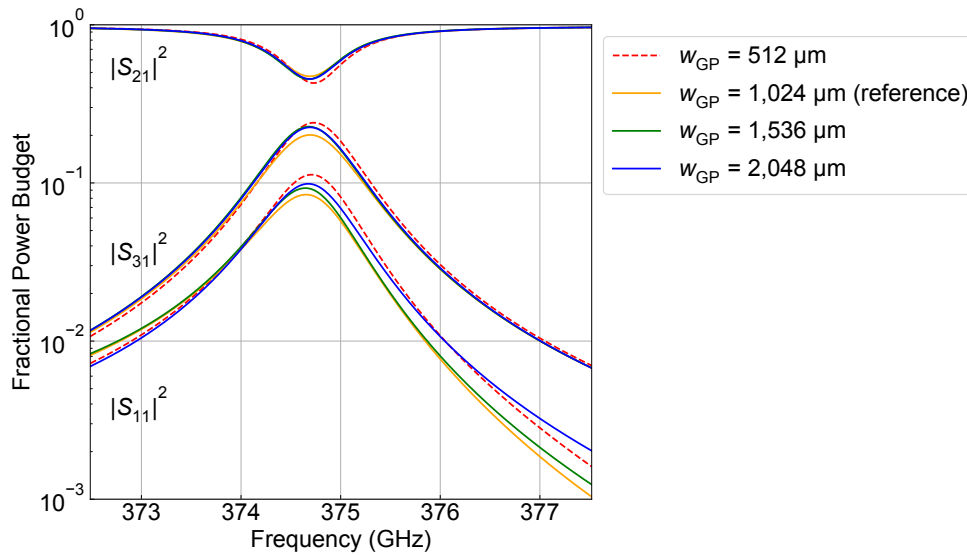

Figure 7. The effect of changing the ground plane width, w_{GP}.

4.4 Sensitivity to the thickness of the lossy substrate

t_{lossySub}	0, 10^0, 10^1, **10^2**, 10^3, 10^4 µm
t_{lossyVac}	10^2 µm
$\tan \delta$	10^{-1}
w_{GP}	1024µm
Δ_x	0
Δ_y	0
box size	4096 µm $\times$ 4096 µm

Table 4. Parameters defining the set of geometries used to test the sensitivity to the thickness of the lossy substrate. Bold characters indicate the *reference* geometry.

The thickness of the artificially introduced lossy substrate, t_{lossySub}, has been varied from 0 to 10^4 µm, as summarized in Table 4. For the 0 µm and 1 µm cases, the *Adaptive Band Synthesis* (ABS) of Sonnet had difficulties in converging after simulating at many frequencies, so eventually the simulation had to be terminated. This is most likely because there was a strong standing wave excited in the box because there was not enough attenuation under the ground plane. This shows the necessity to include this lossy layer, and we will focus on the results of $t_{\text{lossy}} = 10^1$–10^4 µm. Fig. 8 shows the resonance peak for the different lossy-substrate thicknesses. Except for the case where the lossy substrate is the thinnest, $t_{\text{lossySub}} = 10^1$ µm, the results are completely insensitive to varying t_{lossySub}. This is an additional, strong indication that the waves radiated from the vicinity of the resonator are strongly attenuated by the lossy layer, thereby not returning to the circuit and not creating standing waves that affect the results.

Although large values of t_{lossySub} hardly affect the simulation time, we have chosen a minimal value of
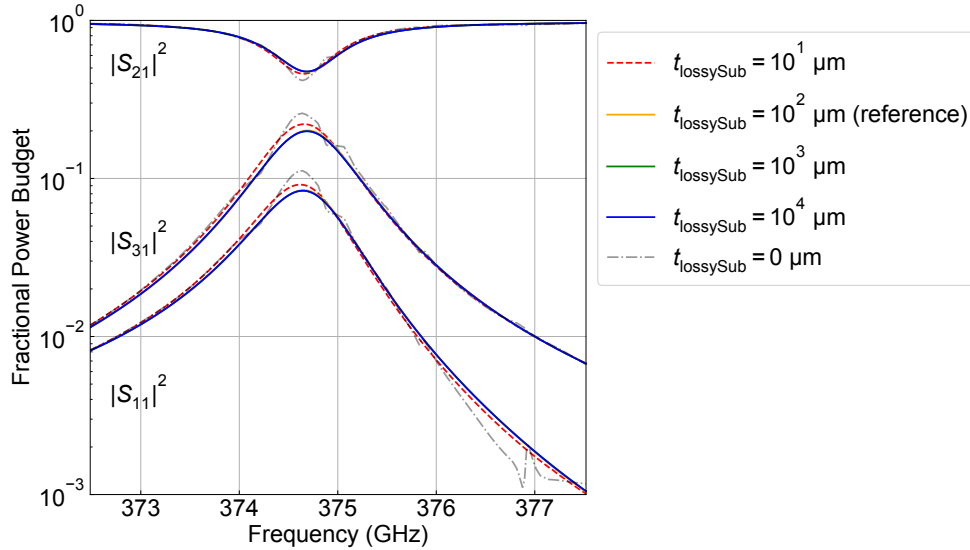
Figure 8. Effect of changing the thickness of the lossy substrate, t_{lossySub}. The three curves for $t_{\text{lossySub}} = 10^2$ µm, 10^3 µm, and 10^4 µm are completely overlapping for all three S-parameters. The curve for $t_{\text{lossySub}} = 0$ µm shows substrate-resonance features, especially at around 375 GHz and 377 GHz.

$t_{\text{lossySub}} = 10^2$ µm as the *reference* value because it is sufficient.

4.5 Sensitivity to the thickness of the lossy vacuum layer

t_{lossySub}	10^2 µm
t_{lossyVac}	0, 10^1, $\mathbf{10^2}$, 10^3, 10^4 µm
$\tan\delta$	10^{-1}
w_{GP}	1024µm
Δ_x	0
Δ_y	0
box size	4096 µm $\times$ 4096 µm

Table 5. Parameters defining the set of geometries used to test the sensitivity to the thickness of the lossy vacuum layer. Bold characters indicate the *reference* geometry.

In a similar way as the previous section, the thickness of the artificially introduced lossy vacuum layer t_{lossyVac} has been varied from 0 to 10^4 µm, as summarized in Table 5. The lossy vacuum layer has no noticeable effect on the results in the case of this model, as shown in Fig. 9. The lossy vacuum layer has no effect on the straight-CPW simulation in section 5 either. This is as expected, because the radiation from these circuits is directed towards the substrate.[16] Moreover, even for geometries that might radiate towards the box ceiling, that radiation could be efficiently absorbed by the free-space boundary because there is no reflective dielectric-vacuum interface in between. Nevertheless, we include the lossy vacuum layer in the box to confirm that there are no standing waves in the volume above the substrate, by an analysis as shown in Fig. 9.

4.6 Sensitivity to the cell size (meshing)

Finally we check that the simulation has a sufficiently small cell size (or mesh size). The *reference* geometry had a cell size of 0.5 µm in both x and y directions. In Fig. 10 we compare the *reference* result with a simulation in which the cell size was reduced to 0.25 µm. Making the cell size smaller shifted the resonance frequency downwards by a factor of 1.0096. In Fig. 10 we have multiplied the frequency of the 0.25 µm result with this factor so that the resonance frequencies match. After this correction, the two sets of curves are nearly overlapping. This result verifies that the *reference* geometry is sufficiently meshed.
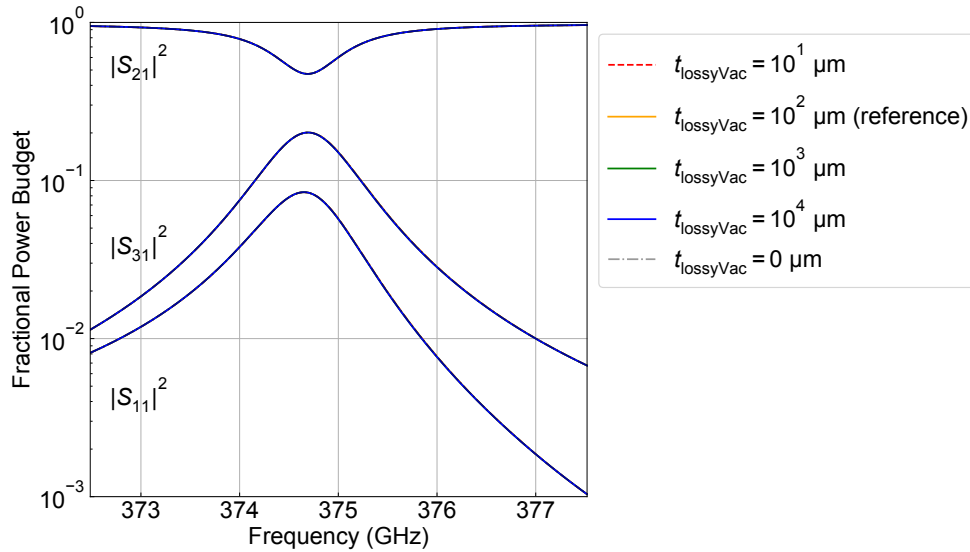
Figure 9. Effect of changing the thickness of the lossy vacuum layer, t_{lossyVac}. The three curves for $t_{\mathrm{lossyVac}} = 10^2$ µm, 10^3 µm, and 10^4 µm are completely overlapping for all three S-parameters.
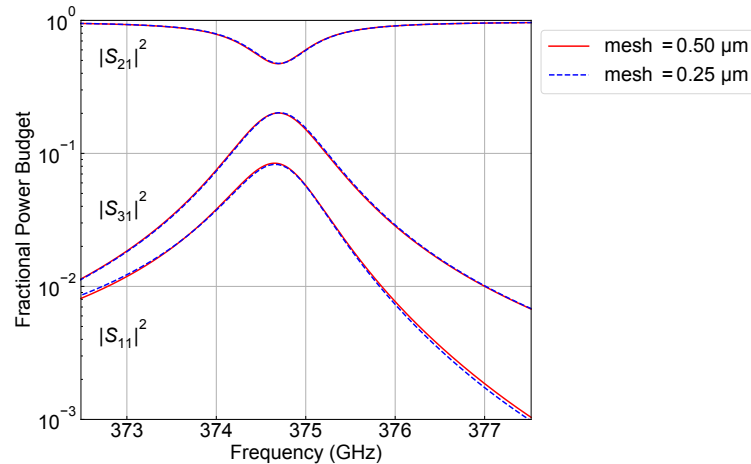

Figure 10. Effect of changing the mesh size, from the *reference* value of 0.5 µm (solid curves) to 0.25 µm (dashed curves) in both x and y directions.

5. SIMULATION OF RADIATION LOSS FROM A STRAIGHT CPW

To show the general applicability of the stratification, we present the simulation of radiation loss from a straight CPW using the same stratification as the one used for the resonator. A similar simulation has been presented in Ref.[11] Here we we will compare the results to the analytical formula of Ref.[17]

We have used Sonnet to simulate the radiation loss of a straight CPW made of PEC with a center strip width of 2 µm and a slot width of 2 µm, on a silicon substrate with a relative dielectric constant of 11.44. The lateral dimensions of the Sonnet box were 3000 µm × 3000 µm. The thicknesses of the layers were the same as those of the *reference* geometry, except for the thickness of the lossy substrate that was varied: $t_{\mathrm{lossuSub}} = 10^2$, 10^3, 10^4 µm. Fig. 11 shows the Sonnet-simulated $|S_{21}^2|$ for different CPW lengths.[11] $|S_{11}^2|$ was < -45 dB with no clear frequency-dependence, which proves that the ports will matched well to the CPW line and reflections are negligible for this analysis. From the slope of a linear-fit to the $|S_{21}^2|$ as a function of frequency, we obtain a loss of 0.030 dB mm^{-1}. This is close to the loss of 0.025 dB mm^{-1} obtained from analytical formula of Frankel et al.:[17]

$$\alpha_{\rm rad} = \left(\frac{\pi}{2}\right)^5 2\left(\frac{\sin^4\Psi}{\cos\Psi}\right)\frac{(s+2w)^2\varepsilon_r^{3/2}}{c^3 K(\sqrt{1-k^2})K(k)}f^3, \tag{1}$$

where α is the attenuation constant, $\Psi = \arccos(\sqrt{\varepsilon_{\rm eff}/\varepsilon_{\rm r}})$ is the radiation angle[11] (see Fig. 12. $90° - \Psi$ is equivalent to the Mach angle for sonic shock waves), $\varepsilon_{\rm eff}$ is the effective dielectric constant of the CPW mode (defined as $\varepsilon_{\rm eff} \equiv \sqrt{(c/v_{\rm p})}$, where $v_{\rm p}$ is the phase velocity), $\varepsilon_{\rm r}$ is the relative dielectric constant of the substrate, s is the width of the center strip of the CPW, w is the width of the CPW slots, c is the velocity of light in vacuum, $k = s/(s+2w)$, f is the frequency, and K is the complete elliptical integral of the first kind. It should be noted that the simulated data has an offset from zero loss at zero distance, most likely due to port discontinuities.
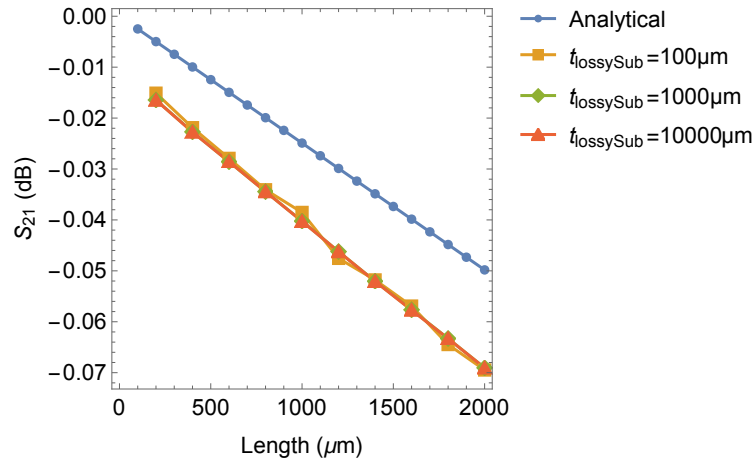

Figure 11. Radiative loss along the $s = w = 2$ μm CPW as a function of length. The analytical line is calculated using Eq. 1. The other curves are calculated using Sonnet, for different thicknesses of the lossy dielectric, $t_{\rm lossySub}$.

The current distribution around the CPW is shown in Fig. 12 (▶ online video). The current propagates away from the CPW, showing no indication of standing waves in the vertical direction. The direction of the shock waves agrees well with $\Psi = \arccos(\sqrt{\varepsilon_{\rm eff}/\varepsilon_{\rm r}}) = 42.5°$.

6. DISCUSSION AND CONCLUSION

Our results show that the 2.5-dimensional MoM solver Sonnet can be used to accurately simulate the radiation loss from planar superconducting circuits, placed in between a thick substrate and vacuum. The Sonnet simulations of the resonator reproduce the $|S_{31}^2|$ measurement result to within the error margin of the measurement. The Sonnet results are robust against variations in the geometric parameters, though it appears to be that changing the parameters studied here lead to a small systematic *increase* in the $|S_{31}^2|$ peak value. This could be an indication that even better accuracy could be reached by studying the effect of the box size and ground plane size, in combination, in greater detail.
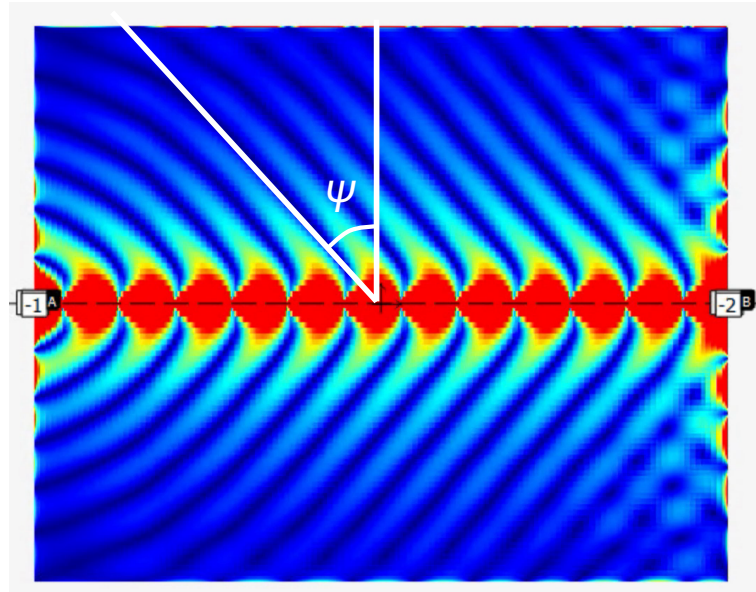
ACKNOWLEDGMENTS

Figure 12. Snapshot of the current distribution J_{xy} around a straight CPW (▶ online video). $\Psi = \arccos(\sqrt{\varepsilon_{\text{eff}}/\varepsilon_{\text{r}}}) = 42.5°$ is derived from $\varepsilon_{\text{eff}} = 6.22$ of the CPW line calculated by Sonnet and $\varepsilon_{\text{r}} = 11.44$ of the Si substrate. Note that the current densities plotted do not represent de-embedded data, and therefore areas near any port include the effect of the port discontinuity, according to the manual of Sonnet.[15]

REFERENCES

[1] Endo, A., Karatsu, K., Tamura, Y., Oshima, T., Taniguchi, A., Takekoshi, T., Asayama, S., Bakx, T. J. L. C., Bosma, S., Bueno, J., Chin, K. W., Fujii, Y., Fujita, K., Huiting, R., Ikarashi, S., Ishida, T., Ishii, S., Kawabe, R., Klapwijk, T. M., Kohno, K., Kouchi, A., Llombart, N., Maekawa, J., Murugesan, V., Nakatsubo, S., Naruse, M., Ohtawara, K., Pascual Laguna, A., Suzuki, J., Suzuki, K., Thoen, D. J., Tsukagoshi, T., Ueda, T., de Visser, P. J., van der Werf, P. P., Yates, S. J. C., Yoshimura, Y., Yurduseven, O., and Baselmans, J. J. A., "First light demonstration of the integrated superconducting spectrometer," *Nature Astronomy* **3**, 989–996 (Aug. 2019).

[2] van Rantwijk, J., Grim, M., van Loon, D., Yates, S., Baryshev, A., and Baselmans, J., "Multiplexed readout for 1000-pixel arrays of microwave kinetic inductance detectors," *IEEE Transactions on Microwave Theory and Techniques* **64**(6), 1876–1883 (2016).

[3] Monfardini, A., Benoit, A., Bideaud, A., Swenson, L., Cruciani, A., Camus, P., Hoffmann, C., Désert, F. X., Doyle, S., Ade, P., Mauskopf, P., Tucker, C., Roesch, M., Leclercq, S., Schuster, K. F., Endo, A., Baryshev, A., Baselmans, J. J. A., Ferrari, L., Yates, S. J. C., Bourrion, O., Macias-Perez, J., Vescovi, C., Calvo, M., and Giordano, C., "A Dual-band Millimeter-wave Kinetic Inductance Camera for the IRAM 30 m Telescope," *Astrophysical Journal Supplement Series* **194**, 24 (June 2011).

[4] Barends, R., Kelly, J., Megrant, A., Veitia, A., Sank, D., Jeffrey, E., White, T. C., Mutus, J., Fowler, A. G., Campbell, B., Chen, Y., Chen, Z., Chiaro, B., Dunsworth, A., Neill, C., O'Malley, P., Roushan, P., Vainsencher, A., Wenner, J., Korotkov, A. N., Cleland, A. N., and Martinis, J. M., "Superconducting quantum circuits at the surface code threshold for fault tolerance," *Nature* **508**(7497), 500–503 (2014).

[5] Bruno, A., de Lange, G., Asaad, S., van der Enden, K. L., Langford, N. K., and DiCarlo, L., "Reducing intrinsic loss in superconducting resonators by surface treatment and deep etching of silicon substrates," *Applied Physics Letters* **106**(18), 182601 (2015).

[6] Driessen, E. F. C., Coumou, P. C. J. J., Tromp, R. R., de Visser, P. J., and Klapwijk, T. M., "Strongly disordered tin and nbtin *s*-wave superconductors probed by microwave electrodynamics," *Phys. Rev. Lett.* **109**, 107003 (Sep 2012).

[7] "Sonnet User's Guide | Sonnet ." http://www.sonnetsoftware.com/support/manuals.asp.

[8] "CST Microwave Studio-3D EM simulation software." https://www.cst.com/products/cstmws.

[9] "High Frequency Structure Simulator (HFSS)." https://www.ansys.com/products/electronics/ansys-hfss.

[10] "How EM Works | Sonnet ." http://www.sonnetsoftware.com/products/sonnet-suites/how-EM-works.html.

[11] Hähnle, S., Marrewijk, N. v., Endo, A., Karatsu, K., Thoen, D. J., Murugesan, V., and Baselmans, J. J. A., "Suppression of radiation loss in high kinetic inductance superconducting co-planar waveguides," *Applied Physics Letters* **116**(18), 182601 (2020).

[12] Noroozian, O., Day, P. K., Eom, B. H., Leduc, H. G., and Zmuidzinas, J., "Crosstalk Reduction for Superconducting Microwave Resonator Arrays," *IEEE Transactions on Microwave Theory Techniques* **60**, 1235–1243 (May 2012).

[13] Wheeler, J., Hailey-Dunsheath, S., Shirokoff, E., Barry, P. S., Bradford, C. M., Chapman, S. C., Che, G., Doyle, S., Glenn, J., Gordon, S., Hollister, M. I., Kovács, A., LeDuc, H. G., Mauskopf, P. D., McGeehan, R., McKenney, C., Reck, T. J., Redford, J., Ross, C., Shiu, C., Tucker, C., Turner, J., Walker, S., and Zmuidzinas, J., "SuperSpec, The On-Chip Spectrometer: Improved NEP and Antenna Performance," *J. Low Temp. Phys.* **84**, 1–7 (May 2018).

[14] Endo, A., Karatsu, K., Laguna, A. P., Mirzaei, B., Huiting, R., Thoen, D. J., Murugesan, V., Yates, S. J. C., Bueno, J., Marrewijk, N. v., Bosma, S., Yurduseven, O., Llombart, N., Suzuki, J., Naruse, M., de Visser, P. J., van der Werf, P. P., Klapwijk, T. M., and Baselmans, J. J. A., "Wideband on-chip terahertz spectrometer based on a superconducting filterbank," *Journal of Astronomical Telescopes, Instruments, and Systems* **5**, 035004 (Jul 2019).

[15] "Plotting Conventions | Sonnet ." http://www.sonnetsoftware.com/support/sonnet/help_topics/plotting_considerations.htm.

[16] Button, K. J., [*Infrared and Millimeter Waves V10: Millimeter Components and Techniques, Part II*], Elsevier (1983).

[17] Frankel, M. Y., Gupta, S., Valdmanis, J. A., and Mourou, G. A., "Terahertz attenuation and dispersion characteristics of coplanar transmission lines," *IEEE Transactions on Microwave Theory and Techniques* **39**(6), 910–916 (1991).